Chemically synthesized gold nanoparticles embedded in a SiO_2 matrix: A model system to give insights into nucleation and growth under irradiation

G. Rizza* and Y. Ramjauny
Ecole Polytechnique, Laboratoire des Solides Irradiés, CEA-DSM-DRECAM/CNRS, 91128 Palaiseau Cedex, France

T. Gacoin and L. Vieille
Ecole Polytechnique, Groupe de Chimie du Solide, Laboratoire de Physique de la Matière Condensée, UMR CNRS 7643, 91128 Palaiseau, France

S. Henry
Centre de Spectrométrie Nuclaire et de Spectrométrie de Masse, CNRS-IN2P3, Bâtiment 108, 91405 Orsay, Campus, France
(Received 27 April 2007; revised manuscript received 13 July 2007; published 13 December 2007)

The control over the size and the dispersion of the ion beam-synthesized nanoparticles is generally poor. This is partially due to the scarce knowledge of the behavior of the precipitate phase in the first stages of the nucleation and growth processes. To overcome this difficulty, we explore the formation and growth under MeV ion irradiation of satellites clusters around chemically synthesized Au particles embedded in a silica matrix. Our results show that the satellites evolve in an Ostwald ripening regime limited by the diffusion in an open system. In addition, the complete evolution of the gold supersaturation is obtained and the temporal window for the nucleation regime is determined. It allows us to give a guideline method to improve the control of the particles monodispersity during the ion beam synthesis. Moreover, an estimation of the threshold concentration for nucleation, an effective value for the surface tension of the Au nanoparticles and the gold diffusivity under irradiation are given.

DOI: 10.1103/PhysRevB.76.245414 PACS number(s): 61.80.Jh, 61.46.−w, 68.37.Lp, 81.07.Bc

I. INTRODUCTION

Ion beam synthesis (IBS) has proved to be a suitable method for obtaining materials based on nanoclusters (NCs). The research activity in this field is stimulated by the possibility to produce high volume fractions of NCs with specific properties and potential applications in nanoelectronics and nanophotonics, see, e.g., Refs. 1–3. However, during ion implantation, the uncontrolled nucleation and growth processes result in broad spatial and size distribution of the nanoparticles. This reduces the possible practical applications.[2,3] Although nucleation and growth during implantation can be controlled to some extent by varying ion flux and substrate temperature, the control of the NCs size distribution remains a challenging task. To overcome this difficulty, new ion-based methodologies have been developed either (i) by combining the electronic energy deposition and the thermal annealing,[5] or (ii) by having recourse to multiple implantation steps and intermediate annealing.[4]

In the present work, the challenge of rationalizing and improving ion beam synthesis of NCs has been studied in detail. In particular, it represents an attempt to go beyond in the description of the nucleation and growth of a precipitate phase under ion irradiation. The final objective is to provide a guideline method to overcome the limitations in controlling the NCs size and spatial distributions that are associated with the ion implantation technique. These limitations are mainly related to the difficulty in performing experiments with an appropriate control of the initial NC conditions, which depend on the complex relation between particle growth through solute depletion, and particle dissolution, induced by displacement cascades triggered by the impinging ions.

Recently, irradiation has been employed as a tool to tailor the properties of nanostructures already present in the matrix or deposited on a surface, e.g., Refs. 6–9 and 15. This sort of *ion beam nanomanipulation* allows, for example, the NCs morphology to be shaped,[6,7] or the nucleation and growth of elements already present in the matrix to be promoted. The latter results in the formation of a halo of satellites around the original NC.[8–15] Here the evolution of the satellite clusters by the MeV-ion irradiation-induced dissolution of gold NCs in a silica matrix has been investigated with a twofold purpose: (i) to study the kinetics of the growth of the satellites (we show that it can be described by a diffusion-limited Ostwald ripening mechanism in an open system) and (ii) to determine the complete evolution of the Au solute concentration as a function of the fluence. It allows one, in principle, to modify the temporal extension of the nucleation regime, and thus the final particles size distribution, by varying in a controlled way both the temperature and the irradiation parameters. Finally, we obtain estimates for: (i) the concentration threshold for precipitation, (ii) the surface tension of the gold particles, and (iii) the diffusion coefficient of the metal atoms within silica under irradiation.

II. EXPERIMENTAL

To obtain an insight into the evolution of a precipitate phase under ion irradiation, not only a control of the irradiation parameters but also of the initial NC properties is required. In this optic, we recently developed a method to prepare samples in a very controlled way. Metallic NCs are first chemically synthesized and then sandwiched between two layers. The details of the chemical synthesis of the nanopar-

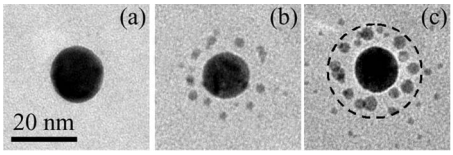

FIG. 1. [(a)–(c)] TEM micrographs of Au NCs irradiated at increasing fluences with 4 MeV Au ions at room temperature. (c) The circle represents an eyeball separation of the areas of growth of the two generations of satellites.

ticles and their confinement into the host matrix have been reported elsewhere.[15]

Special care must be taken to obtain an accurate description of the kinetic evolution of the satellites. In particular, it is crucial that the initial depth and size distributions of the pristine NCs are as narrow as possible. The former condition is related to the necessity that all particles evolve in the same energy loss regime. This condition is satisfied if the NCs are embedded at the same depth from the sample surface. The latter condition depends on the fact that the NCs size influences the satellites growth.[16] In fact, in a previous work we observed that, for a given fluence, the mean size of the satellites scales with the size of the pristine NC.[16] Our preparation method avoids these difficulties because nearly monodispersed chemically synthesized NCs are grafted onto the surface of a first matrix layer before being coated by a second layer.

For the present study 15 ± 2 nm Au NCs are embedded within a 500 nm silica layer. All the Au NCs are in a plane at 200 nm below the surface of the silica film. The samples were irradiated at room temperature and under a constant ion flux 1 μA cm^{-2} with 4 MeV Au ions using the ARAMIS accelerator,[17] of the CSNSM laboratory (Orsay, France). The nuclear energy loss for Au ions into Au NCs (S_n $=7.5$ keV nm^{-1}) as well as their implantation depth into the matrix ($R_p\sim1\pm0.1$ μm) were estimated using the SRIM2006 code.[18,19] R_p is at least five times the depth at which the NCs were introduced (200 nm). Hence the implanted Au does not interact with the Au NCs.

Finally, some comments are necessary to define the fluence range. Recently, Rizza *et al.* observed that the evolution of the satellites can be described by a two-step process:[15] (i) for low irradiation fluences (up to about $2-3\times10^{16}$ cm^{-2}) satellites are observed to grow, directly sustained by the NC dissolution and (ii) for fluences higher than about 4×10^{16} cm^{-2}, when the pristine NC is below a critical size, the satellites are partially dissolved by the irradiation. Thus, to describe the satellite kinetics we limit our investigation to the first regime, i.e., for fluences up to 2.2×10^{16} cm^{-2}.

The characterization of the samples was performed by transmission electron microscopy (TEM) with a 300 keV Philips CM30. The average size, the size distribution, and the spatial distribution of the Au NCs were obtained in planar transmission electron microscopy (P-TEM), Fig. 1. The transmission electron microscopy micrographs were processed with a slow-scan CCD camera and analyzed with the digital micrograph program.

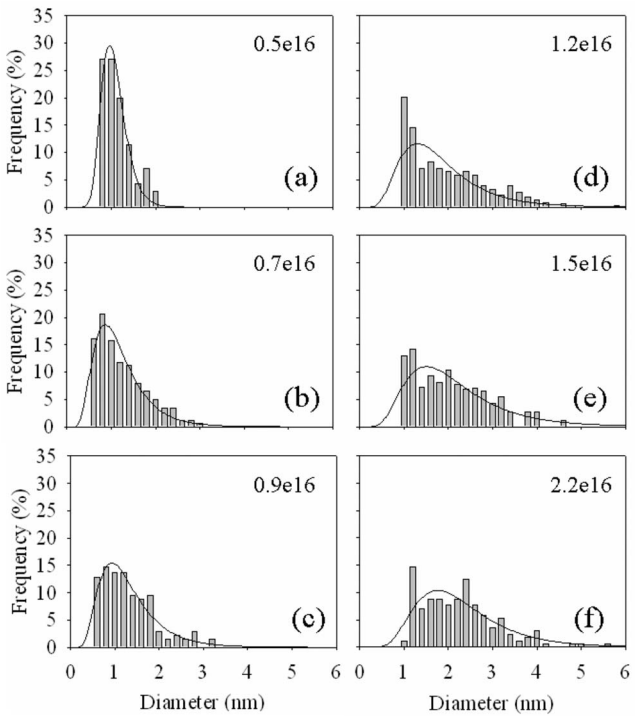

FIG. 2. Size distributions of satellites as a function of the irradiation fluence.

III. RESULTS

Figure 1(a) shows a planar-view TEM micrograph of an as-prepared Au NC. Irradiation favors the formation of a halo of satellite clusters around each pristine NC, Figs. 1(b) and 1(c). For our TEM conditions, the minimum resolvable particle size is estimated to be about 0.5 nm. In a previous work,[15] we have shown that (i) at low irradiation fluences, a *first generation* of satellites nucleate close to the NC surface, where the latter is considered a solute reservoir Fig. 1(b) and (ii) for higher irradiation fluences, a *second generation* of satellites nucleates at increasing distances from the NC surface, when supersaturation created by both the NC and the first generation of satellites overcomes a threshold value, Fig. 1(c). As the satellites close to the NC surface are systematically larger than those far from it, we limited our investigation to the evolution of the first ones, those close to the NC. Experimentally they are found within an annular region around the NC with a thickness ranging between 1 and 1.5 times the NC radius.

A simply electron diffraction analysis indicates that the fcc crystallographic structure of the NCs is not modified by the irradiation. Nonetheless, it is worth noting that very recently, Kluth *et al.*[13] using a more sophisticated EXAFS spectroscopy analysis showed that irradiation induces disorder in the crystalline nanophase.

Figures 2(a)–2(f) show the evolution of the satellite size distribution (SSD) as a function of the irradiation fluence. The distributions are normalized to the number of satellites, i.e., the ordinate corresponds to their frequency of appearance, and fitted with a lognormal function using the average particle size and the standard deviation as parameters. Two

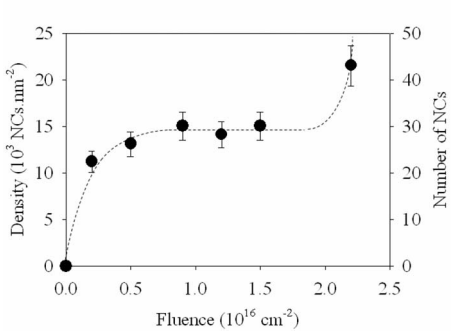

FIG. 3. Evolution of the satellite density with irradiation fluence.

different behaviors can be distinguished: (i) the broadening of the SSD and, for larger fluences, the corresponding peak shift toward larger sizes, and (ii) the decrease of the nucleation frequency, i.e., the reduction of the number of satellites smaller than 1 nm. For example, at 0.5×10^{16} cm^{-2} about 60% of the particles have a size less or equal to 1 nm. This value is reduced to about 20% at 1.2×10^{16} cm^{-2}, and less than 5% for a fluence of 2.2×10^{16} cm^{-2}.

Figure 3 shows the evolution of the satellite density. After a short transient regime a steady-state value of about 15×10^{-3} particles nm^{-2} is reached for fluences larger than 0.5×10^{16} cm^{-2}. Finally, above 1.5×10^{16} cm^{-2} a further increase is observed.

In Fig. 4 we report the evolution of the average satellite size with fluence, $R(\Phi)$. The experimental data have been interpolated using the power function $R(\Phi)=a\Phi^b$. The best fit for this function gives a proportionality coefficient of $a=0.74\pm0.04$ and a time exponent of $b=0.37\pm0.03$, respectively. The corresponding correlation coefficient is $\Re=0.99$.

Hence, to summarize we have shown that the evolution of the satellites under MeV irradiation is characterized by (i) a constant reduction of the nucleation rate, (ii) a steady-state value of the satellite density at least up to a fluence of 1.5×10^{16} cm^{-2}, and (iii) growth kinetics of the type $R(\Phi)\sim\Phi^{0.37\pm0.03}$.

IV. DISCUSSION

The study of the NCs growth kinetics is virtually impossible with the ion implantation technique, due to the high

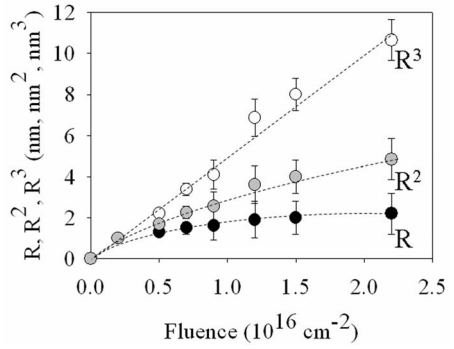

FIG. 4. Evolution of the satellites mean size (R), square (R^2), and cube (R^3) as a function of the irradiation fluence.

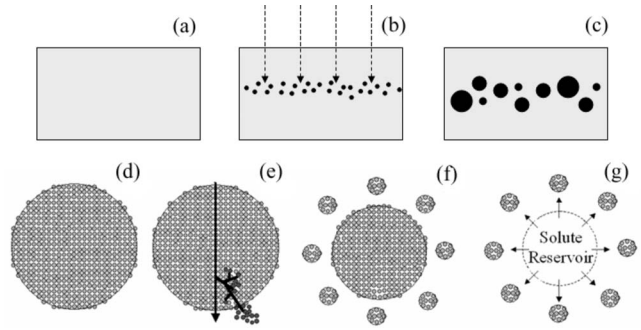

FIG. 5. Schematic representation of [(a)–(c)] implantation and [(d)–(g)] nanoimplantation. (g) In an open system the NC can be replaced by a fictive solute reservoir.

fluence necessary to induce the precipitation, e.g., for gold in silica an implantation fluence larger than 10^{17} cm^{-2} is needed.[20] However, MeV irradiation of preimplanted samples allows one to reduce the threshold implantation dose for nucleation by at least two orders of magnitude.[21] In our experimental setup ion irradiation is used with a double purpose: (i) to promote the gold solute deposition into the silica matrix through the irradiation-induced NCs dissolution and (ii) to enhance the satellites nucleation by reducing the nucleation threshold. This allows the precipitation to be observed already at a fluence of 10^{15} cm^{-2} and the evolution of the precipitate phase to be easily investigated. The basic idea of our approach is that the physics underlying the precipitation and growth of a second phase during ion implantation is equivalent to those that intervene during the satellites nucleation and growth [Figs. 5(a)–5(f)]. Here high solute concentration is deposited in small volumes around the NC, via the irradiation-induced displacement cascades. We call this process *nanoimplantation*. Thus, studying the evolution of the satellite clusters under nanoimplantation is a way to gain insight into the mechanisms of nucleation and growth under ion implantation.

A. Theory

To describe the precipitation and growth under irradiation the classical nucleation and growth theory can be used.[22,23] The key parameter is the supersaturation $S(t)$ defined as $S(t)=[C(t)-C_\infty]/C_\infty$, where $C(t)$ is the solute concentration at a given time and C_∞ is the bulk solubility. However, although the satellite nucleation and growth is directly sustained by the dissolution of the original NC, its evolution can be described in two ways: (i) The ensemble composed of the original NC and the surrounding satellites can be considered as a "closed system," i.e., the external flux of matter is zero. In such a "conservative system," the irradiation allows the total mass of the pristine Au particle to be spatially redistributed over a larger *fixed* volume containing also the satellites. (ii) The evolution of the satellites can be described as produced by an external monomer supply. In this case, the original NC, acting as a solute source, can be replaced by a fictive solute reservoir as shown in Fig. 5(g). Here, the satellite precipitation occurs in a finite region with open mass ex-

change with neighboring regions of different concentration. As, in principle, the two choices are equally appropriate, we extend the formulation of the particle growth by considering both closed and open systems. Depending on $S(t)$, the phase separation in a supersaturated solid solution can—both for closed and open systems—be divided into distinct stages.

1. Supersaturation regime

As soon as the solute is introduced into the host matrix, e.g., during ion implantation or nanoimplantation, $S(t)$ increases linearly as a function of the amount of monomers deposited. This goes on up to a critical value S_c, at a time t_1, after which spontaneous nucleation sets in. It is worth noting that due to the fact that ion-implantation or nanoimplantation are nonequilibrium processes it is possible to introduce concentrations of dopants into a solid matrix that are much higher than the equilibrium dopant solubility. Thus S_c is generally higher than the bulk solubility, i.e., $S=1$.

2. Nucleation regime

When the solute concentration $S(t)$ exceeds S_c, stable embryos start to form. Owing to the occurrence of nucleation and subsequent growth of the nuclei (e.g., the precipitates act as a sink for the diffusing solute), $S(t)$ starts to decrease despite the ongoing monomer deposition, and the supersaturation eventually drops below the nucleation threshold at a time t_2. The region between t_1 and t_2 is usually referred to as the *nucleation* region.

3. Growth regime

Below S_c, the nucleation of new particles is inhibited and all the existing NCs grow by incorporating the incoming monomers. Hence, the number of the particles reaches a steady-state value:[27] $N(t) \sim$ const. Conversely, the diffusion of monomers to the particle interface and their absorption *via* the interface reaction drives the NCs growth. The kinetic laws are (i) limited by the diffusion, if the monomer absorption is the faster process or (ii) limited by the interface kinetics, if the monomer diffusion is the faster process. A general expression for the particle growth rate, valid for both closed and open systems, writes[24,25]

$$\frac{dR}{dt} = \frac{KC_\infty \Lambda_C}{R_C}\left(\frac{1 - R_C/R}{1 + \epsilon R}\right), \tag{1}$$

where R is the particle radius, K is the rate of monomer absorption at the particle surface, σ is the surface tension, $R_C = \Lambda_C / S(t)$ is the critical particle radius, Λ_C is the capillarity length, $\epsilon^{-1} = D_0 V a / \mathrm{K}$ is the screening length, D_0 is the diffusion coefficient, and V_a is the molar volume.

In Eq. (1) the factor $\epsilon R = KR / D_0 V a$ determines the dominating mechanism. When $KR \ll D_0 V a$, the growth is limited by the reaction interface and for $R \gg R_C$,[26] the number of particles and the particle radius scale as

$$N \propto \text{const}, \tag{2a}$$

$$R \propto t. \tag{2b}$$

When $KR \gg DV_A$ the growth is limited by the diffusion of the monomers. Considering the asymptotic solution ($R \gg R_C$) the number of particles and the particle radius evolve as

$$N \propto \text{const}, \tag{3a}$$

$$R \propto t^{0.5}. \tag{3b}$$

4. Ostwald ripening regime

When the supersaturation reaches a sufficiently low value, the smaller particles become instable and eventually dissolve, since the critical radius of the particles scales as the inverse of the supersaturation level, i.e., $R_C \propto 1/S(t)$. This regime is called *Ostwald ripening* (OR). The evolution of a precipitate phase in the OR regime is different for closed and open systems.

(a) In *closed systems* the mass is conserved. The supersaturation cannot remain constant indefinitely and thus decreases with the time. The system evolves towards a redistribution of the mass that minimizes the total free energy. Interface effects become important and the smaller precipitates dissolve in favor of the larger ones. The description of the evolution of the particles in an OR regime was originally developed by Lifshitz, Slyozov[28] and Wagner[29] and is nowadays knows as the LSW theory.

If the monomer assimilation is limited by the *interface reaction* the precipitates size and number evolve as

$$R \propto t^{0.5}, \tag{4a}$$

$$N \propto t^{-1.5}. \tag{4b}$$

On the other hand, for surface absorption limited by the *diffusion of the monomers* one has

$$R \propto t^{0.33}, \tag{5a}$$

$$N \propto t^{-1}. \tag{5b}$$

(b) In an *open system*, the continuous monomer supply allows the particle dissolution to be reduced, or eventually stopped. This mechanism is called *Ostwald ripening in an open system* or *second independent growth* (SIG).[30] In an open system the kinetic laws are the same as for the particles evolving under mass conservation. However, the scaling law for the number of particles is different and depends on the absorption mechanism.[30,31]

If the monomer absorption is limited by the *surface reaction* the particle size and number evolve as

$$R \propto t^{0.5}, \tag{6a}$$

$$N \propto t^{-0.5}. \tag{6b}$$

On the other hand, in the *diffusion-limited* regime they evolve as

$$R \propto t^{0.33}, \tag{7a}$$

$$N \propto \text{const}. \tag{7b}$$

TABLE I. Evolution of the radius and the number of the precipitate phase within the regimes of growth and coarsening within closed and open systems.

	Growth regime		Ostwald ripening regime	
	Close system	Open system	Close system	Open system
Interface kinetics limited regime	$R \propto t$	$R \propto t$	$R \propto t^{0.5}$	$R \propto t^{0.5}$
$(KR \ll DV_A)$	$N \sim$ const	$N \sim$ const	$N \sim t^{-1.5}$	$N \sim t^{-0.5}$
Diffusion limited regime	$R \propto t^{0.5}$	$R \propto t^{0.5}$	$R \propto t^{0.33}$	$R \propto t^{0.33}$
$(KR \gg DV_A)$	$N \sim$ const	$N \sim$ const	$N \sim t^{-1}$	$N \sim$ const

B. Kinetic evolution of satellites

The mechanism controlling the evolution of an ensemble of particles in a supersaturated solid solution can be characterized knowing (i) the size distribution function $f(R(\Phi))$, (ii) the change of the particle radii with time, $R(\Phi)$, and (iii) the evolution of the number of particles, $N(\Phi)$.

De Lamaëstre *et al.*[32] have recently shown that when ion implantation is involved, the nucleation and growth history of the clusters is no longer revealed by the distribution function, which often evolves towards a lognormal shape. As the kinetic evolution of the second phase does not lead to the predicted distribution shape, experimental distributions cannot be used to discriminate among different regimes. Conversely, the other two quantities $R(\Phi)$ and $N(\Phi)$ are experimentally accessible. First, we analyze the evolution of the average particle radius with fluence, $R(\Phi)$. The time t is linearly related to the fluence *via* the constant ion flux φ i.e., $\Phi = \varphi t$. In the Results section we showed that the fluence exponent for satellite growth is 0.37 ± 0.03, as can be seen in Fig. 4. According to the theoretical predictions summarized in Table I, any possible link with the growth regime can be ruled out since the particle size scales as $R \sim t$, for the reaction-limited, and as $R \sim t^{0.5}$, for the diffusion-limited kinetics. Moreover, the OR regime governed by interface reactions can also be excluded as the satellite sizes scale as $R \sim t^{0.5}$. Hence, both for closed or open systems the time exponent can only correspond to OR within a diffusion-limited regime. To discriminate between the two options, we look at the evolution of the number of satellites, $N(\Phi)$ (Fig. 3). After a rapid increase at the beginning of the irradiation, $N(\Phi)$ reaches a steady-state value up to a fluence of 1.5×10^{16} cm^{-2}, then it starts to increase. This depends on the fact that for higher irradiation fluences the original NC can no longer be considered as an infinite solute reservoir.[15] As inspection of Table I reveals, the only mechanism accounting for our experimental results, $R(\Phi) \sim \Phi^{0.37}$ and $N(\Phi) \sim$ const, is the *OR regime in an open system, i.e., under a monomer supply that is diffusion limited.*

To conclude this section we can say that when the embedded NC can be considered as an infinite solute source, i.e., for low irradiation fluences, the second phase precipitation can be studied by subdividing the problem into two parts: (i) the irradiation-induced NC dissolution, i.e., the evolution of the solute reservoir, and (ii) the particle growth under external monomer supply. In the latter case the classical nucleation and growth theory can be applied.

C. Nucleation fraction

In this section we analyze the evolution of the nucleation fraction with irradiation, $n(\Phi)$. It is obtained from satellite size distributions (Fig. 2), by normalizing the number of satellites with radius smaller than 1 nm to their total number, $N(\Phi)$. The result is shown in Fig. 6(a). The experimental data can be fitted with an exponential decay function, indicating that the nucleation of new satellites decreases with the irradiation.

$$n(\Phi) = a * \exp(-b\Phi). \tag{8}$$

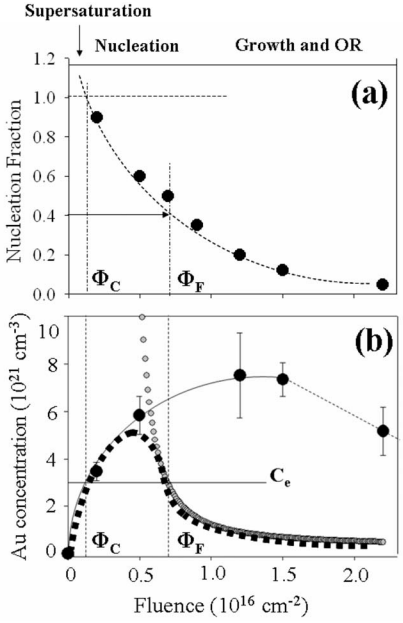

FIG. 6. (a) Evolution of the nucleation fraction of the satellites with fluence, i.e., the fraction of satellites smaller than 1 nm. (b) The evolution of the Au solute concentration with fluence can be estimated by considering two opposite terms: (i) The full black circles represent the continuous monomers addition into the matrix due to the irradiation-induced NC dissolution. (ii) The full gray circles represent the evolution of solute concentration into the matrix above the nucleation threshold. The difference between the two curves is related to the amount of solute which is absorbed by the growing nanoparticles. Finally, the dashed line describes the complete evolution of the Au solute concentration with fluence.

The best fit is obtained for $a=1.22$ and $b=0.145\times10^{-15}$ at.$^{-1}$ cm^2. The corresponding correlation coefficient is $\Re=0.998$. Several parameters can be determined from the inspection of Fig. 6(a): (i) the fluence threshold for nucleation, Φ_C, (ii) the fluence corresponding to the end of the nucleation regime, Φ_F, and (iii) the time-dependent nucleation rate. Φ_C corresponds to the condition $n=1$, i.e., all the particles have a size smaller than 1 nm, and is given by $\Phi_C\sim0.16\times10^{16}$ cm^{-2}. Of course it represents an upper limit of the threshold fluence for nucleation. Φ_F can be estimated as the characteristic length of Eq. (8), i.e., $\Phi_F=1/b\sim0.68\times10^{16}$ cm^{-2}. The nucleation rate $dn(\Phi)/d\Phi$ can be used to determine the change of the supersaturation with irradiation and will be calculated in the following sections.

D. Estimation of the concentration threshold for satellites nucleation

Nucleation is expected to set in when the solute concentration exceeds a nucleation threshold c_e. In the previous section we estimated the critical fluence for nucleation to be $\Phi_c=0.16\times10^{16}$ cm^{-2}. During irradiation an original NC is progressively dissolved. The number of atoms displaced into the silica matrix at Φ_c is simply given by $\Delta N(\Phi_c)=c_p\Delta V^{NC}_{\Phi_c}=1.6\times10^4$ at. Here $c_p=5.9\times10^{22}$ at cm^{-3} is the gold bulk density and $\Delta V^{NC}_{\Phi_c}=4/3\pi[R^3(0)-R^3(\Phi_c)]$ is the NC dissolved volume at Φ_c as measured from TEM micrographs. Once in solution, the Au atoms can diffuse over a volume ΔV^{sat} before precipitation occurs. The latter is experimentally estimated from TEM micrographs as the volume containing the satellites at $\Phi_c, \Delta V^{sat}_{\Phi_C}\sim5.6\times10^{-18}$ cm^3. Thus, an upper limit of c_e can be evaluated to be

$$c_e = c_p\frac{\Delta V^{NC}_{\Phi_C}}{\Delta V^{sat}_{\Phi_C}} \sim 2.8\times10^{21} \text{ at cm}^{-3}. \tag{9}$$

In Eq. (9) all the parameters are experimentally determined with the exception of the NC atomic density C_p, defined as the bulk density for gold. Although C_p could be modified by the intermixing of the matrix recoils (Si and/or O), several elements can be given to justify the validity of our approximation: (i) SRIM simulations show that the implantation depth of Si and O into Au is nearly limited to the very first NC surface. (ii) Irradiation-induced vacancies aggregation and voids formation already observed in other systems, e.g., Ref. 20, were not evidenced by our TEM analysis. (iii) Extended X-ray-absorption fine structure (EXAFS) measurements indicate that preimplanted impurities, Si and O atoms (10% at.), into an Au film do not affect its atomic structure when irradiated with 2.3 MeV Sn ions.[13]

In the literature only few estimations of the nucleation threshold exist. Ila *et al.*[20] found that an upper limit of c_e for gold in silica at 1200 °C is below $c_e<9\times10^{21}$ at cm^{-3}. Recently, Ramaswamy *et al.*[4] calculated the variation of c_e for temperatures ranging between 500 °C and 800 °C. These are reported in Fig. 7 (full circles) together with our estimation at room temperature (open circles). The dotted line is simply the extrapolation of c_e towards the low temperature regime. Clearly our estimation agrees reasonably well with the data of Ref. 4.

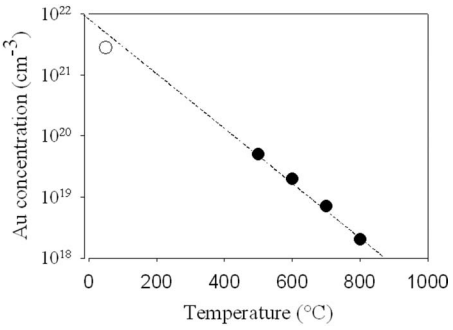

FIG. 7. The full circles represent the experimental threshold values for gold nucleation in silica within the temperature range 500–800 °C, as taken from Ref. 4. The extrapolation of these to lower temperatures is given by the dotted line. The open circles represent our estimates at room temperature.

E. Evolution of the solute concentration with fluence

The evolution of the solute concentration with irradiation depends on two opposite terms: (i) the continuous addition of monomers, which is due to the NC dissolution and which enhances the metal concentration within the host matrix and (ii) the absorption of monomers into the forming and the growing particles, which favors the decrease of the total amount of available solute.

The first term can be calculated as in the previous section, where now the dissolved volume of the NC and the annular region containing the satellites are determined for all the irradiation fluences.

$$c(\Phi) = c_p\frac{\Delta V^{NC}(\Phi)}{\Delta V^{sat}(\Phi)}. \tag{10}$$

The evolution of the solute concentration with fluence is shown in Fig. 6(b), the full black circles. Here, the concentration of dissolved monomers increases with fluence up to 1.5×10^{16} cm^{-2} and then decreases. In a previous work, we showed that when the size of the original NC becomes comparable to that of the surrounding satellites each particle turns into an equivalent solute source and a regime change occurs in the satellites evolution.[15] Hence, the reduction of the solute concentration, associated with the observation of the increasing of the satellite density for fluences larger than 1.5×10^{16} cm^{-2}, clearly indicates that a new regime is active and that the original NC can no longer be considered as an infinite solute source.

The second term, corresponding to the solute concentration above the fluence threshold for nucleation, $\Phi>\Phi_c$, can be calculated using the classical nucleation theory as follows:[23,34]

$$I(t) = I_0\exp\left[\frac{-B}{(\ln S(t))^2}\right], \tag{11}$$

where $I(t)$ is the nucleation rate, I_0 is the maximum nucleation rate, $S(t)$ is the supersaturation, $B=16\pi\sigma^3V_a^2/3(kT)^3$, σ

is the surface tension, V_A is the molar volume, k is Boltzmann's constant, and T is the temperature. Rearranging Eq. (11), the supersaturation $S(t)$ writes

$$S(t) = \exp\left[\frac{-B}{2\ln(I/I_0)}\right]. \quad (12)$$

The evolution of the gold supersaturation in silica matrix is found by equating the relative nucleation rate I/I_0 to the experimental one, I^{exp}/I_0^{exp}. I^{exp} is obtained by differentiating Eq. (8), $I^{exp}=\dot{n}(\Phi(t))$, and the maximum experimental nucleation rate is given by $I_0^{exp}=\dot{n}(\Phi_C)\varphi=4.4\times10^{-4}$ s^{-1}, where $\dot{n}(\Phi_C)\simeq1.4\times10^{-16}$ cm^2 and $\varphi=3.12\times10^{12}$ at cm^{-2} s^{-1}. We obtain

$$S(\Phi) = \exp\left[\frac{B}{2b(\Phi-\Phi_C)}\right], \quad (13)$$

where $b=0.145\times10^{-15}$ at.$^{-1}$ cm^2 and $\Phi_C=0.16\times10^{16}$ cm^{-2}. Finally, an expression for the solute concentration is obtained by multiplying Eq. (13) by the equilibrium concentration, C_∞

$$C(\Phi) = S(\Phi)C_\infty = \exp\left[\frac{8\pi\sigma^3V_a^2}{3b(kT)^3(\Phi-\Phi_C)}\right]C_\infty, \quad (14)$$

where $kT=5\times10^{-21}$ J and $V_a=1.6\times10^{-23}$ cm^3. The only two unknown parameters of Eq. (14) are the equilibrium concentration C_∞ and the surface tension σ. However, a condition for the fit is imposed by the fact that the nucleation regime ends at $\Phi=\Phi_F$, where the supersaturation must be $C(\Phi_F)=C_e$. The best fit for Eq. (14) is given in Fig. 6(b), the full gray circles. The surface tension has been estimated to be in the range of $\sigma\sim1-2.2\times10^{-5}$ J cm^{-2}. It is worth noting that this slight variation is obtained by changing the equilibrium concentration over orders of magnitude, e.g., $10^{10}-10^{21}$ cm^{-3}.

The combination of Eq. (10) and Eq. (14) represents the complete evolution of the solute concentration with irradiation, i.e., the dashed line in Fig. 6(b). The supersaturation regime crosses over into the nucleation regime at a fluence of about $\Phi_C\sim0.16\times10^{16}$ cm^{-2}, and it turns into the growth regime for fluences higher than $\Phi_F\sim0.68\times10^{16}$ cm^{-2}.

The possibility to estimate the evolution of the supersaturation with fluence allows us to study how the irradiation parameters modify the nucleation and growth regimes. It is clear that when the nucleation window is temporally large the final size distribution will be broad, because the particles can nucleate (and grow) at different times. On the other hand, the shorter the nucleation regime, the narrower the final particles dispersion, as all the particles nucleate (and grow) at almost the same time. Thus, a way to tailor the final size distribution of the precipitates is to modify the nucleation window by varying in a controlled way both the temperature and the irradiation parameters.

F. Surface tension of the gold nanoparticles under irradiation

The surface tension of ion-beam-synthesized gold NCs embedded in a silica matrix has been estimated by several authors. A value of 4×10^{-4} J cm^{-2} was extrapolated by De Marchi *et al.*[33] from TEM measurements. Values of 3.6 $\times10^{-4}$ J cm^{-2} (Ref. 35) and 3.4×10^{-4} J cm^{-2} (Ref. 36) were deduced by Kluth *et al.* form EXAFS experiments using a simple liquid-drop model.[38] All these results are in good agreement with those obtained for freestanding NCs, suggesting a negligible influence of the silica matrix, e.g., Buffat *et al.*[37] give 1.38×10^{-4} J cm^{-2}, whereas Balarena *et al.*[38] obtain 3.46×10^{-4} J cm^{-2}. However, our value is one order of magnitude lower than the previous ones, $1-2.2\times10^{-5}$ J cm^{-2}. Thus, in the following we try to account for this discrepancy.

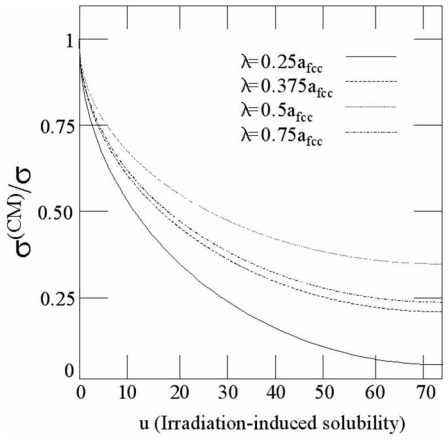

FIG. 8. Monte Carlo simulation showing the decrease of the surface tension under irradiation σ^{MC} with respect to the equilibrium value σ, as a function of the ballistic force u, for different values of the mixing length λ, from Ref. 39.

There is a crucial difference between our experiment and the former ones in as far as the experimental setup is concerned:

(i) In all the previous works, gold NCs precipitate during the post-implantation annealing treatment, i.e., the nanoparticles grow under purely thermal conditions.

(ii) In our case, gold NCs form by the irradiation-induced dissolution of the gold particles and by solute reprecipitation in their surroundings, i.e., the nanoparticles grow under irradiation conditions.

It is evident that irradiation drives the irradiated system away from its equilibrium state. This is due to the forced atomic relocation induced by nuclear collision. In other words, the displacement cascades perturb the equilibrium conditions at the particle surface modifying the value of the surface tension. This effect has been nicely described by Strobel *et al.*[39] using the K3DLMC code. In Fig. 8 the ratios of values of the surface tension under irradiation $\sigma^{(CM)}$, to their values within the purely thermal case σ, are represented as a function of the mixing length, i.e., the average distance at which monomers are displaced from the NC surface, and the ballistic force u, i.e., the strength of the solute source. The ratio $\sigma^{(CM)}/\sigma$ decreases as the source strength, i.e., the u parameter is increased.

Heinig *et al.*[40] have recently shown that the asymptotic expression for the steady-state concentration of a NC under irradiation takes an expression equivalent to that of Gibbs-Thomson: $C^I(R)=C_\infty^I(R)(1+R_C^I/R)$, where C^I and R_C^I are, respectively, the equilibrium solute concentration at planar sur-

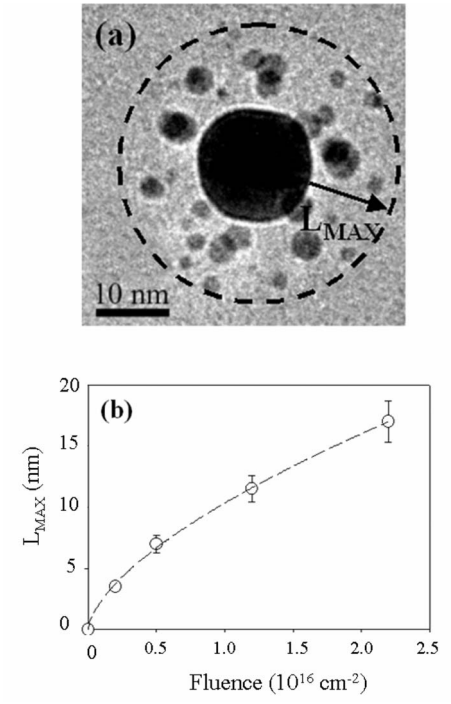

FIG. 9. (a) Bright-field image of a sample irradiated with a fluence of 1×10^{16} cm^{-2}. The maximum satellite-clusters distance is indicated by the dotted circle (b). Increase of the maximum satellite-clusters distance (as calculated from the original cluster surface) as a function of the fluence of the irradiating ions.

face and the capillarity length under irradiation. The model predicts that irradiation reduces the surface tension, i.e., the value of the capillarity length R_C^I, and that for appropriate irradiation conditions an effective negative value of the surface tension can be achieved. Similar conclusions have been drawn by other recent theoretical studies.[41,42]

Although additional work is needed to clarify the influence of the ion-matter interaction on the decrease of the surface tension, our estimation represents the experimental determination of the effective surface tension of gold NCs under irradiation.

G. Diffusion coefficient under irradiation, D_{red}

Rizza *et al.*[15] have shown that the diffusion coefficient under irradiation, D_{red}, can be qualitatively related to the maximum distance at which satellites were found, L_{max},[43–45]

$$D_{red} = \frac{L_{max}^2 \varphi}{\Phi}, \tag{15}$$

where Φ is the irradiation fluence and φ is the constant ion flux. Using this expression, here we provide a quantitative estimation for D_{red}.

In Fig. 9 the evolution of $L_{max}(\Phi)$ with the fluence is shown. The experimental data are fitted with the function,

$$L_{max} = a\Phi^{0.5}, \tag{16}$$

where $a=(D_{red}/\varphi)^{0.5}=0.6$ nm is the free parameter and $\varphi=3.12\times10^{-2}$ ions s^{-1} nm^{-2}. Thus the diffusion coefficient under irradiation is simply given by

$$D_{red} = a^2\varphi \simeq 3.8\times10^{-16}\ \text{cm}^2\ \text{s}^{-1}. \tag{17}$$

De Marchi *et al.*[33] estimated the diffusion coefficient during postimplantation annealing experiments at 900 °C to be $D\sim5\times10^{-17}$ cm^2 s^{-1}. On the other hand, Rizza *et al.*[8] give a crude estimation of D_{red} based on the ratio of thermal to irradiation-enhanced diffusion and the ion-beam-induced displacement rate deduced from the SRIM code, $D\sim1.5\times10^{-16}$ cm^2 s^{-1}. Our estimation is comparable to the latter. This may be related to the amount of defects created by the irradiation, enhancing the atomic mobility more efficiently than in the purely thermal case. This is consistent with Martin's model,[46] which states that a solid solution under irradiation at temperature T (and flux φ) is equivalent to the one evolving at an higher effective temperature, i.e., $T^{irr}=T[1+\Delta(T,\varphi)]$. Thus we can conclude that the diffusivity of the gold solute under MeV Au ions irradiation at room temperature corresponds to a fictive temperature above 900 °C.

V. CONCLUSION

The way one must follow to improve the final particle monodispersity is to separate the nucleation and growth processes. The new ion-based methodologies operate within this direction. However, their main limitations are related to our poor knowledge of the behavior of the precipitate phase in the first stages of the nucleation, which prevents the possibility to precisely control the final particle properties. This work was motivated by the ambition to fill this gap and represents a first step in the quantitative description of the precipitation process as obtained through ion implantation.

In summary, using Au colloids embedded in a silica matrix as a model system and considering the original NC as a fictive solute source, we show that the evolution of the precipitate phase under irradiation is successfully described by an Ostwald ripening mechanism in an open system limited by the diffusion. Moreover, we estimate the concentration threshold for nucleation as well as the surface tension and the gold diffusivity in silica under irradiation. To conclude, our approach makes it possible to assess the evolution of the (*nano-*)*implanted* solute with the irradiation, in particular, the extent of the nucleation regime. In this respect, further experiments are scheduled to modify this regime in a controlled way by playing both with the irradiation parameters and with the temperature. The final key issue is the optimum control of the nanostructures, when these are synthesized with ion-beam-related techniques.

ACKNOWLEDGMENTS

We gratefully acknowledge L. Delbecq and C. Boukari for their contribution to this work.

*giancarlo.rizza@polytechnique.edu

[1] *Handbook of Nanostructured Materials and Nanotechnology*, edited by F. Gonella and P. Mazzoldi (Academic Press, San Diego, 2000), Vol. 4.
[2] A. Meldrum, L. A. Boatner, and C. W. White, Nucl. Instrum. Methods Phys. Res. B **178**, 7 (2001).
[3] P. Mazzoldi and G. Mattei, Riv. Nuovo Cimento **28**, 1 (2005).
[4] V. Ramaswamy, T. E. Haynes, C. W. White, W. J. Roorda, and M. J. Aziz, Nano Lett. **5**, 373 (2005).
[5] E. Valentin, H. Bernas, C. Ricolleau, and F. Creuzet, Phys. Rev. Lett. **86**, 99 (2001).
[6] E. Snoeks, A. van Bladeeren, T. van Dillen, C. M. van Kats, M. L. Brongersma, and A. Polman, Adv. Mater. (Weinheim, Ger.) **12**, 1511 (2000).
[7] J. J. Penninkhof, T. van Dillen, S. Roorda, C. Graf, A. van Bladeeren, A. M. Vredenberg, and A. Polman, Nucl. Instrum. Methods Phys. Res. B **242**, 523 (2006).
[8] G. C. Rizza, M. Strobel, K. H. Heinig, and H. Bernas, Nucl. Instrum. Methods Phys. Res. B **178**, 78 (2001).
[9] G. Mattei, G. De Marchi, C. Maurizio, P. Mazzoldi, C. Sada, V. Bello, and G. Battaglin, Phys. Rev. Lett. **90**, 085502 (2003).
[10] G. Mattei, G. Battaglin, V. Bello, G. De Marchi, C. Maurizio, P. Mazzoldi, M. Parolin, and C. Sada, J. Non-Cryst. Solids **322**, 17 (2003).
[11] V. Bello, G. De Marchi, C. Maurizio, G. Mattei, P. Mazzoldi, M. Parolin, and C. Sada, J. Non-Cryst. Solids **345**, 685 (2004).
[12] G. Mattei, V. Bello, P. Mazzoldi, G. Pellegrini, C. Sada, C. Maurizio, and G. Battaglin, Nucl. Instrum. Methods Phys. Res. B **240**, 128 (2005).
[13] P. Kluth, B. Johannessen, G. J. Foran, D. J. Cookson, S. M. Kluth, and M. C. Ridgway, Phys. Rev. B **74**, 014202 (2006).
[14] P. Kluth and M. C. Ridgway, Nucl. Instrum. Methods Phys. Res. B **242**, 458 (2006).
[15] G. Rizza, H. Cheverry, T. Gacoin, A. Lamasson, and S. Henry, J. Appl. Phys., **101**, 014321 (2007).
[16] G. Rizza, Y. Ramjauny, T. Gacoin, and S. Henry, Nucl. Instrum. Methods Phys. Res. B **257**, 15 (2007).
[17] E. Cottereau, J. Camplan, J. Chaumont, R. Munier, and H. Bernas, Nucl. Instrum. Methods Phys. Res. B **45**, 293 (1990).
[18] J. F. Ziegler, J. P. Biersack, and U. Littmark, *The Stopping Ranges and Ranges of Ions in Solids* (Pergamon Press, New York, 1985).
[19] http://www.srim.org
[20] D. Ila, E. K. Williams, S. Sarkisov, C. C. Smith, D. B. Poker, and D. K. Hensley, Nucl. Instrum. Methods Phys. Res. B **141**, 289 (1998).
[21] D. Ila, E. K. Williams, R. L. Zimmerman, D. B. Poker, and D. K. Hensley, Nucl. Instrum. Methods Phys. Res. B **166**, 845 (2000).
[22] *Phase Transformations in Metals and Alloys*, 2nd ed., edited by D. A. Porter and K. E. Easterling (Nelson Thornes, Cheltenham, UK, 2001).
[23] *Growth and Coarsening*, edited by L. Ratke and P. W. Voorhees (Springer, New York, 2002).
[24] I. H. Leubner, J. Phys. Chem. **91**, 6069 (1987).
[25] K. Nozawa, M.-H. Delville, H. Ushiki, P. Panizza, and J.-P. Delville, Phys. Rev. E **72**, 011404 (2005).
[26] In the growth regime the supersaturation is still relatively high, thus, R_C can be very small and a stable embryo can be composed by only a few atoms. In this regard, EXAFS measurements indicate that Au atoms, displaced from the Au NC into the silica matrix by 2.3 MeV Sn ions, can form very small clusters composed by only dimers, trimers,… (Ref. 13). As in our experiment $R > 0.5$ nm, e.g., larger than the smallest resolvable nanoparticle, the condition $R \gg R_C$ is satisfied.
[27] M. Strobel, K. H. Heinig, W. Möller, A. Meldrum, D. S. Zhou, C. W. White, and R. A. Zuhr, Nucl. Instrum. Methods Phys. Res. B **147**, 343 (1999).
[28] I. M. Lifshitz and V. V. Slyozov, J. Phys. Chem. Solids **19**, 35 (1961).
[29] V. C. Wagner, Z. Elektrochem. **65**, 581 (1961).
[30] E. Brosh and A. Kiv, J. Nucl. Mater. **306**, 173 (2002).
[31] F.-P. Ludwig and J. Schmelzer, Z. Phys. Chem. **192**, 155 (1995).
[32] R. Espiau de Lamaëstre and H. Bernas, Phys. Rev. B **73**, 125317 (2006).
[33] G. De Marchi, G. Mattei, P. Mazzoldi, C. Sada, and A. Miotello, J. Appl. Phys. **92**, 4249 (2002).
[34] *Kinetics of Materials*, edited by R. W. Balluffi, S. M. Allen, and W. C. Carter (Wiley, New York, 2005).
[35] P. Kluth, B. Johannessen, V. Giraud, A. Cheng, C. J. Glover, G. de M. Azevedo, and M. C. Ridgway, Appl. Phys. Lett. **85**, 3561 (2004).
[36] P. Kluth, B. Johannessen, D. J. Cookson, G. J. Foran, and M. C. Ridgway, Nucl. Instrum. Methods Phys. Res. B **246**, 30 (2006).
[37] Ph. Buffat and J-P. Borel, Phys. Rev. A **13**, 2287 (1976).
[38] A. Balarena, E. Bernieri, P. Picozzi, A. Reale, S. Santucci, E. Burattini, and S. Mobilio, Surf. Sci. **156**, 156 (1985).
[39] M. Strobel, Ph.D. thesis, FZR, Dresden, 1999.
[40] K. H. Heinig, T. Müller, B. Schmidt, M. Strobel, W. Möller, Appl. Phys. A: Mater. Sci. Process. **77**, 17 (2003).
[41] R. A. Enrique and P. Bellon, Phys. Rev. B **63**, 134111 (2001).
[42] J.-W. Liu and P. Bellon, Phys. Rev. B **66**, 020303(R) (2002).
[43] *Ion-Solids Interactions Fundamentals and Applications*, edited by M. Nastasi, J. W. Mayer, and J. K. Hirvonen (Cambridge University Press, Cambridge, UK, 1996).
[44] H. Hosono and N. Matsunami, Nucl. Instrum. Methods Phys. Res. B **141**, 566 (1998).
[45] J. C. Pivin, G. Rizza, F. Garrido, and L. Thom, Europhys. Lett. **39**, 623 (1997).
[46] G. Martin, Phys. Rev. B **30**, 1424 (1984).